Human Molecular Genetics, 2020, Vol. 29, No. 15 2508–2522

doi: 10.1093/hmg/ddaa138
Advance Access Publication Date: 3 July 2020
General Article

GENERAL ARTICLE

Correction of cilia structure and function alleviates multi-organ pathology in Bardet–Biedl syndrome mice

Hervé Husson[1,†,*], Nikolay O. Bukanov[1,†,‡], Sarah Moreno[1,§], Mandy M. Smith[1], Brenda Richards[2], Cheng Zhu[2], Tyler Picariello[1], Hyejung Park[3], Bing Wang[3], Thomas A. Natoli[1], Laurie A. Smith[1], Stefano Zanotti[1], Ryan J. Russo[1,‖], Stephen L. Madden[2], Katherine W. Klinger[2], Vijay Modur[4] and Oxana Ibraghimov-Beskrovnaya[1,¶]

[1]Rare and Neurologic Diseases Research, Sanofi, Framingham, MA 01701, USA, [2]Translational Sciences, Sanofi, Framingham, MA 01701, USA, [3]Pre-Development Sciences, Sanofi, Waltham, MA 02451, USA and [4]Rare Diseases Development, Sanofi, Cambridge, MA 02142, USA

*To whom correspondence should be addressed. Tel: +1 5082702217; Fax: +1 5082714955; Email: herve.husson@sanofi.com

Abstract

Bardet–Biedl syndrome (BBS) is a pleiotropic autosomal recessive ciliopathy affecting multiple organs. The development of potential disease-modifying therapy for BBS will require concurrent targeting of multi-systemic manifestations. Here, we show for the first time that monosialodihexosylganglioside accumulates in *Bbs2*$^{-/-}$ cilia, indicating impairment of glycosphingolipid (GSL) metabolism in BBS. Consequently, we tested whether BBS pathology in *Bbs2*$^{-/-}$ mice can be reversed by targeting the underlying ciliary defect via reduction of GSL metabolism. Inhibition of GSL synthesis with the glucosylceramide synthase inhibitor Genz-667161 decreases the obesity, liver disease, retinal degeneration and olfaction defect in *Bbs2*$^{-/-}$ mice. These effects are secondary to preservation of ciliary structure and signaling, and stimulation of cellular differentiation. In conclusion, reduction of GSL metabolism resolves the multi-organ pathology of *Bbs2*$^{-/-}$ mice by directly preserving ciliary structure and function towards a normal phenotype. Since this approach does not rely on the correction of the underlying genetic mutation, it might translate successfully as a treatment for other ciliopathies.

[†]These authors contributed equally to this study.
[‡]Present address: Janssen Pharmaceutical, 4 Blackfan Circle, Boston, MA 02115, USA.
[§]Present address: MiMedx, 1775 West Oak Commons Ct. NE, Marietta, GA 30062, USA.
[‖]Present address: Alnylam, 675 W Kendall St, Cambridge, MA 02142, USA.
[¶]Present address: Dyne Therapeutics, 830 Winter St, Waltham, MA 02451, USA.

Received: May 15, 2020. **Revised:** June 22, 2020. **Accepted:** July 1, 2020

Introduction

Ciliopathies are a class of disorders caused by genetic mutations that result in the abnormal formation or function of cilia. Cilia are highly conserved microtubule-based organelles surrounded by membrane that project from the surface of most vertebrate cell type (1). Cilia functions as antennae to sense environmental cues and link them to key signaling pathways (2,3). Ciliopathies may present clinically as organ-specific disorders or pleiotropic conditions and can manifest with obesity, retinal degeneration, renal cystic disease and cerebral anomalies. Ciliopathies are complex genetic diseases with 187 genes linked to 35 established ciliopathies defined by various phenotypes. In addition, different mutations in the same gene can result in multiple, clinically distinct phenotypes. (2). The pathobiological mechanisms underlying the heterogeneity of these diseases remain largely unknown (4).

Bardet–Biedl syndrome (BBS) is a rare autosomal recessive ciliopathy characterized by obesity, anosmia, retinal degeneration with rod-cone dystrophy, postaxial polydactyly, hypogonadism and renal cystic disease. The genetic variability associated with BBS translates into high phenotypic variations. To date, mutations in 21 *BBS* genes are considered causative (5–7). The encoded proteins are involved in ciliary function, intracellular transport and in multiple protein–protein interactions (5,8–10). Eight BBS proteins (BBS1, BBS2, BBS4, BBS5, BBS7, BBS8, BBS9 and BBS18) assemble a stable complex known as the BBSome, which regulates protein trafficking to the ciliary membrane (11,12). BBS6, BBS10 and BBS12 constitute a chaperonin complex that is important for the proper assembly of the BBSome (13). BBS3 is essential for BBSome recruitment to the membrane and entrance into cilia (14). The partially overlapping functions of BBS proteins are consistent with the phenotypic similarities observed with mutations in distinct *BBS* genes (15,16).

Sphingolipids and glycosphingolipids (GSL) are important regulators of key cellular processes including proliferation, differentiation, signal transduction and modulation of immune responses. GSLs were shown to play crucial roles in cancer progression and in the development of inflammatory, neurological, immune and metabolic disorders (17–20). Recent data demonstrate that GSLs are also central constituents of cilia structure and contribute to ciliary signaling. The GSL monosialodihexosylganglioside (GM3) is a ganglioside enriched in the ciliary membrane of epithelial cells, while ceramide (the precursor to GSL synthesis) appears highly enriched in the centrosomal/pericentriolar cellular compartment (21,22). Interestingly, ciliary length and lipid flux to the cilium may be regulated by the amount of ceramide at the cilia base, such that an increase in ceramide levels favors ciliogenesis (23).

We hypothesized that modulating ciliary signaling defects by modulating GSLs using a small molecule inhibitor of GCS could be beneficial in multi-organ ciliopathies such as BBS. Here, we show for the first time a GSL pathway imbalance in *Bbs2*$^{-/-}$ mice, characterized by accumulation of GM3 in morphologically stunted cilia. Modulation of GSL metabolism in *Bbs2*$^{-/-}$ mice with the administration of the brain-penetrant GCS inhibitor (GCSi) Genz-667161 improves multiple disease manifestations, including obesity, anosmia and retinal degeneration. Mechanistic studies show that the therapeutic effects of Genz-667161 are mediated by preservation of ciliary length and signaling that lead to a restoration of cellular differentiation in the adipose tissue and the olfactory and retinal epithelium towards a normal phenotype. The effects of Genz-667161 in adipose tissue appear driven by a generalized normalization of gene expression in adipocytes.

Results

GCS inhibition normalizes ciliary GM3 expression in *Bbs2*$^{-/-}$ kidney epithelial cells

GSLs are important components of ciliary structure and signaling (21,22). To characterize the impact of the *Bbs2* deletion on ciliary GSL metabolism, we generated a mouse model of BBS harboring the homozygous deletion of exons 5–13 in the *Bbs2* (*Bbs2*$^{-/-}$) locus (Supplementary Material, Fig. S1A), as previously described (16). Quantitative reverse-transcription-polymerase chain reaction (qRT PCR) showed absence of *Bbs2* mRNA when probed with a primer pair and probe set spanning exon 12–13. It is of interest that the *Bbs2* mRNA was increased when probed with a primer pair and probe set spanning exon 16–17, and this effect most likely results from a compensatory mechanism in response to *Bbs2* loss of function (Supplementary Material, Fig. S1B).

Subsequently, we measured ciliary GM3 expression and assessed GM3 ciliary localization in kidney epithelial cell lines generated from *Bbs2*$^{-/-}$ mutants and wild-type (WT) mice. Immunofluorescence (IF) analysis of acetylated tubulin and GM3 co-localization revealed that cilia of *Bbs2*$^{-/-}$ cells exhibited higher GM3 content and were shorter than cilia in WT cells (Fig. 1B and C). In agreement with these results, LC-MS/MS analysis of whole cell lysates demonstrated that GM3 accumulates in *Bbs2*$^{-/-}$ cells and that Genz-667161 prevented this effect also increasing cilia length (Fig. 1B–D and Supplementary Material, Table S1).

GCS inhibition reduces metabolic abnormalities in the *Bbs2*$^{-/-}$ mouse model

To determine the impact of GCS inhibition on the metabolic abnormalities of BBS, *Bbs2*$^{-/-}$ mice were fed a diet containing Genz-667161 (0.033% weight/weight) from 1 to 6 months of age. *Bbs2*$^{-/-}$ mice fed a normal diet served as controls for disease progression. In agreement with previous reports, *Bbs2*$^{-/-}$ mice were smaller than WT littermates at birth (16). Although this difference was no longer noted at 2 months of age, body fat content was higher in 2-month-old *Bbs2*$^{-/-}$ mutants than in WT littermates as shown in the 1 to 6 months longitudinal study (Supplementary Material, Fig. S2 and corresponding Supplementary Material, Table S3). Three-month-old *Bbs2*$^{-/-}$ mice were heavier and displayed higher body fat content than WT littermates, and GCSi administration attenuated these differences up to 6 months of age (Fig. 2A and corresponding Supplementary Material, Table S2; Supplementary Material, Fig. S2 and corresponding Supplementary Material, Table S3). Our findings confirm previous work demonstrating that *Bbs2*$^{-/-}$ mice, like BBS patients, develop obesity and indicate that GCS inhibition may normalize body weight and body fat content in the context of BBS (5,16).

Obesity in BBS is thought to originate both from abnormalities in the central nervous system (CNS) and peripheral adipose tissue (24). Ciliary defects in the hypothalamus of BBS patients inhibit the response to leptin, leading to hyperphagia and increased serum leptin levels. These manifestations of BBS were reproduced in *Bbs2*$^{-/-}$ mice (Fig. 2A and corresponding Supplementary Material, Table S2; Supplementary Material, Fig. S2 and corresponding Supplementary Material, Table S3) and confirmed previous observations in similar models (25–27). Genz-667161 reduced food consumption and serum leptin levels in *Bbs2*$^{-/-}$ mice, suggesting that the CNS defects were

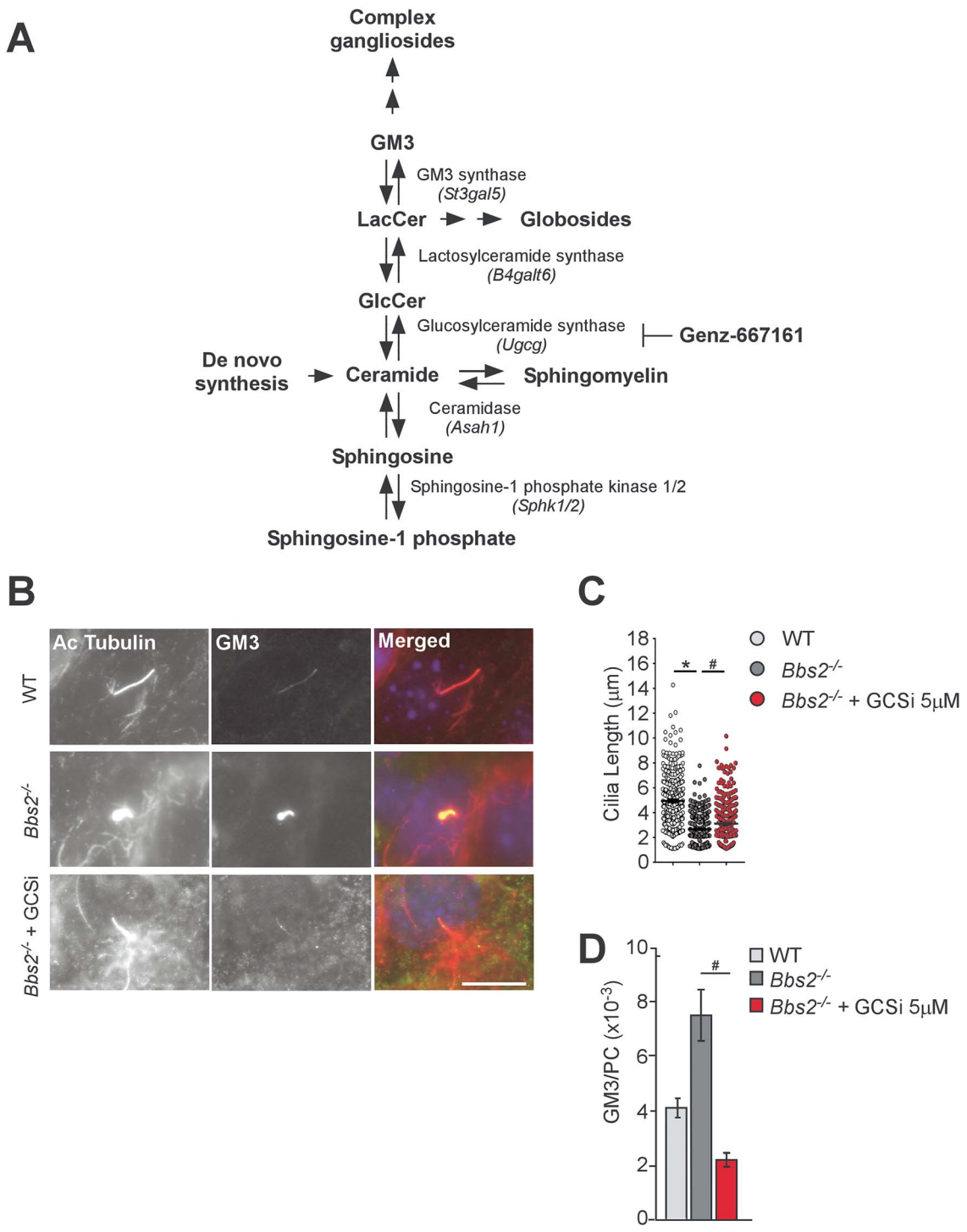

Figure 1. Genz-667161 normalizes GSL distribution in immortalized *Bbs2*$^{-/-}$ kidney epithelial cells. (**A**) Schematic representation of GSL metabolism. The *de novo* synthesis is a multistep process resulting in synthesis of ceramide. Ceramide can be deacylated by ceramidase to sphingosine, or converted to a membrane lipid sphingomyelin, or, alternatively, glycosylated by glucosylceramide (GlcCer) synthase (GCS) to GlcCer. GlcCer can be converted to lactosylceramide (LacCer) by addition of galactose. GlcCer can be further modified to GM3 by GM3 synthase. Genz-667161 is a GCSi. Ceramide can also be converted to sphingosine-1 phosphate, a signaling SL, by the action of ceramidase and by sphingosine kinase 1 or 2 on sphingosine. Gene names are indicated in parentheses. (**B**) Immunofluorescence analysis of GM3 localization in WT immortalized kidney epithelial cells, and *Bbs2*$^{-/-}$ immortalized kidney epithelial cells either treated with 5 μM of GCSi or ethanol (vehicle). Cell cultures were stained for GM3 (green), Ac. Tubulin (red) and nuclei stained with DAPI (blue). Scale bar: 10 μm. (**C**). Quantitation of mean cilia length in WT and *Bbs2*$^{-/-}$, and *Bbs2*$^{-/-}$ cell lines treated with GCSi. WT $N = 357$ cilia, *Bbs2*$^{-/-}$ $N = 350$ cilia, *Bbs2*$^{-/-}$ + GCSi $N = 377$ cilia. (**D**) GM3 levels measured by LC–MS analysis in immortalized kidney epithelial cells from WT and *Bbs2*$^{-/-}$ kidneys. GM3 levels shown are normalized to phosphatidylcholine (PC) level. * indicates $P < 0.05$ WT versus *Bbs2*$^{-/-}$, # indicates $P < 0.05$ *Bbs2*$^{-/-}$ versus *Bbs2*$^{-/-}$ + GCSi; error bars indicate SEM.

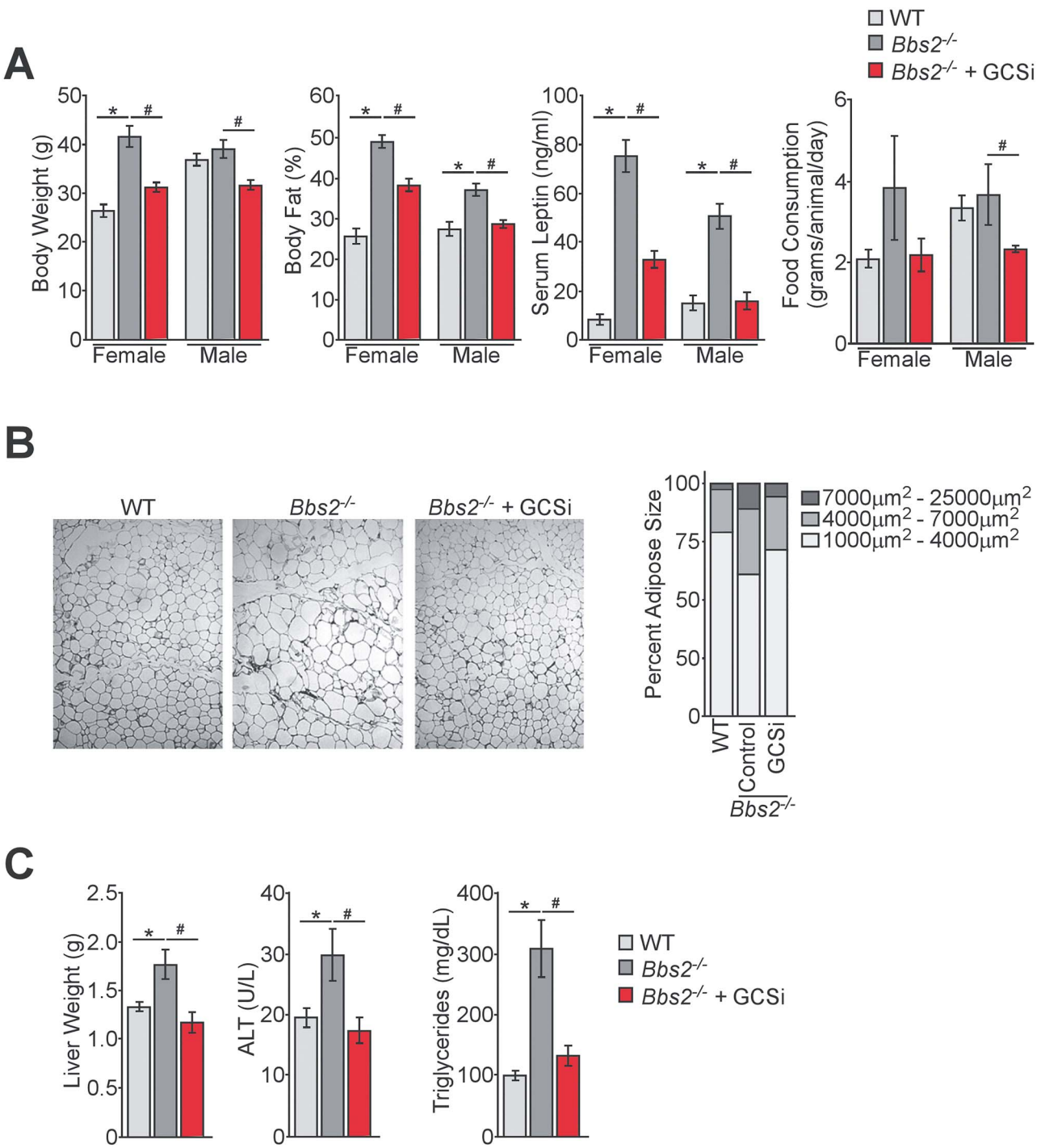

Figure 2. Genz-667161 attenuates the metabolic abnormalities in *Bbs2*$^{-/-}$ mice. (**A**) Changes in metabolic parameters including body weight, body fat percentage, serum leptin and food consumption were measured in 6-month-old WT and *Bbs2*$^{-/-}$ mice, and *Bbs2*$^{-/-}$ littermates treated with GCSi (*Bbs2*$^{-/-}$ + GCSi). (**B**) Representative H&E-stained white adipose tissue (left) and quantification of adipocyte size (right). (**C**) Changes in parameters of liver function including liver weight, serum ALT and serum triglycerides were measured in male WT and *Bbs2*$^{-/-}$ mice, and *Bbs2*$^{-/-}$ littermates treated with GCSi. * indicates $P < 0.05$ WT versus *Bbs2*$^{-/-}$, # indicates $P < 0.05$ *Bbs2*$^{-/-}$ versus *Bbs2*$^{-/-}$ + GCSi; error bars indicate SEM.

reversed by GCS inhibition (Fig. 2A and corresponding Supplementary Material, Table S2; Supplementary Material, Fig. S2 and corresponding Supplementary Material, Table S3). Accordingly, examination of primary cilia structure in the hypothalamus revealed a loss of hypothalamic cilia in *Bbs2*$^{-/-}$ mice that was reduced by GCSi treatment (Supplementary Material, Fig. S3A).

Histological analysis of adipose tissue revealed that adipocytes had greater heterogeneity and were larger in *Bbs2*$^{-/-}$ mice than in WT littermates, an effect that is suggestive of adipocyte hypertrophy in *Bbs2*$^{-/-}$ mutants (Fig. 2B). Cell-size-distribution analysis indicated that adipocyte size was normalized by GCSi treatment (Fig. 2B). As reported in BBS

patients (28), *Bbs2*$^{-/-}$ mice exhibited several liver abnormalities including elevated liver weight, which was reduced to WT levels with GCSi treatment. Serum alanine transaminase (ALT) and triglycerides were significantly increased albeit within normal range in *Bbs2*$^{-/-}$ mice and were reduced to WT levels by GCS inhibition (Fig. 2C and corresponding Supplementary Material, Table S4). As reported previously in a similar *Bbs2* null mouse model, Bbs mice described here do not develop kidney pathology (16).

GCS inhibition corrects anosmia by preserving cilia structure and signaling

The loss of BBS proteins results in anosmia in both humans and mice due to defects in the structure and function of olfactory cilia (16,29). To determine whether anosmia in *Bbs2*$^{-/-}$ mice was improved by GCS inhibition, olfaction was assessed with a functional test based on length of time required to find a buried treat (latency time). In accordance with the anosmia of BBS patients and previous findings in mice, *Bbs2*$^{-/-}$ mutants displayed up to a 5-fold increase in latency time compared to WT controls (Fig. 3A and Supplementary Material, Table 6) (16,29).

We sought out to assess the effect of GCSi on main olfactory epithelium (MOE) cilia and cellular differentiation of underlying cells. We observed a significant reduction of cilia-specific IF staining in the MOE of *Bbs2*$^{-/-}$ mice (Fig. 3B). Moreover, the MOE of *Bbs2*$^{-/-}$ mice displayed significantly decreased amount of adenylate cyclase III (ACIII), the enzyme that initiates the odorant signaling cascade, an effect that was consistent with reduced sensory function (Fig. 3C).

To investigate the effects of GCS inhibition on cellular differentiation in the MOE, we conducted IF analysis of cytokeratin 14 (CK14), SRY-Box 2 (Sox2), doublecortin (Dcx) and olfactory marker protein (OMP), which are protein markers of horizontal basal cells, globose/supporting cells, immature neurons and mature neurons, respectively. *Bbs2*$^{-/-}$ mice displayed an accumulation of Dcx-positive immature neurons at the expense of OMP-positive mature neurons, whereas no differences were noted in basal or supporting cells. Genz-667161 preserved the cellular composition of the MOE, suggesting that GCS inhibition prevented the detrimental effects of *Bbs2* inactivation on the MOE by maintaining neuronal differentiation (Fig. 3D).

GCS inhibition preserved retinal structure in *Bbs2*$^{-/-}$ mice

To establish the effects of GCS inhibition on the vision defects that characterize BBS, we conducted IF analysis of rhodopsin and cone arrestin in retina sections. In agreement with the early-onset blindness that afflicts BBS patients and *Bbs2* null mouse models, *Bbs2*$^{-/-}$ mice presented early-onset severe degeneration of the outer nuclear layer (ONL) characterized by reduced number of rods and cones in the retina (Fig. 4A and B) (16,30). The ONL was significantly thinner in 4-week-old *Bbs2*$^{-/-}$ mice (data not shown) compared to WT controls, and the difference became more pronounced at 6 months of age (Fig. 4A). Genz-667161 administration resulted in an approximate 2-fold increase in the thickness of the ONL (Fig. 4A and Supplementary Material, Table S7) and reinstituted partial expression of cone arrestin, suggesting that GCS inhibition improved the architecture of the retina (Fig. 4B).

GCS inhibition normalizes GlcCer expression in serum and multiple tissues in *Bbs2*$^{-/-}$ mice

To document the efficacy of GCS inhibition, the pharmacodynamics of GSL lowering was assessed by measuring GlcCer levels in serum and multiple tissues. Compared to untreated *Bbs2*$^{-/-}$ mice, up to 90% of GlcCer reduction was achieved in serum and visceral tissues of mice administered with Genz-667161, whereas ~25% reduction in GlcCer levels was observed in brain (Supplementary Material, Fig. S3B and Supplementary Material, Table S5). These data indicated that the reported effects of GCSi inhibition are secondary to reduction of GlcCer.

GCS inhibition normalizes gene expression signatures of adipogenesis, ciliogenesis and GSL pathways in white adipose tissue from *Bbs2*$^{-/-}$ mice

To determine the mechanisms whereby GCS inhibition corrects the adipogenic defect of *Bbs2*$^{-/-}$ mice, we performed next-generation RNA-sequencing (RNA-seq) in white adipose tissue (WAT) from WT mice and *Bbs2*$^{-/-}$ littermates, either fed normal chow or a diet supplemented with Genz-667161. Principal component analysis (PCA) demonstrated that two principal components accounted for ~55% variability in gene expression and were sufficient to segregate *Bbs2*$^{-/-}$ mutants from WT littermates and *Bbs2*$^{-/-}$ mice administered Genz-667161 (Supplementary Material, Fig. S4A). Volcano plots identified a cluster of genes upregulated (red dots) in *Bbs2*$^{-/-}$ compared to WT whose expression was normalized by GCS inhibition (Supplementary Material, Fig. S4B).

Ingenuity pathway analysis (IPA) confirmed that pathways relevant to BBS pathobiology were dysregulated in *Bbs2*$^{-/-}$ mice. More specifically, the glutathione-mediated detoxification pathway was suppressed, whereas FCγ receptor-mediated phagocytosis, natural killer cell signaling, Th1 and Th2 activation and B Cell activation pathways were induced in *Bbs2*$^{-/-}$ mice compared to WT littermates (Fig. 5A). In agreement with our *in vivo* observations, IPA revealed that Genz-667161 attenuated these defects, providing a mechanistic explanation for the reduction of the adipogenic defect by GCS inhibition in *Bbs2*$^{-/-}$ mice (Fig. 5B). Next, we analyzed the expression of key genes involved in the adipogenesis (Fig. 5C and Supplementary Material, Table S8), ciliogenesis (Fig. 5D and Supplementary Material, Table S9) and GSL (Fig. 5E and Supplementary Material, Table S10) pathways. The analysis revealed increased *Lep* and decreased *Cdk5* in the adipogenesis pathway; increased *Bbs2*, *Ift80* and *Arl13B* and decreased *Arl6*, *Ahi1*, *Wdpcp* and *Ift43* in the ciliogenesis pathway; and increased *Ugcg* and *B4galt6*, and decreased *St3gal5* in the GSL pathway. These data show that GCSi normalizes key pathways dysregulated in adipose tissue of *Bbs2*$^{-/-}$ mice.

GCS inhibition decreases adipogenesis triggered by BBS1, BBS2 and BBS10 knockdown in human preadipocytes cultures

More than 21 BBS mutations have been characterized to date, and mutations in *BBS1*, *BBS2* and *BBS10* account for ~50% of all BBS cases (31,32). Therefore, we sought to determine whether GCS inhibition also affects the metabolic abnormalities in other BBS variants, including those caused by BBS1 or BBS10 loss of function. To this end, we tested the effects of Genz-667161 in primary human preadipocytes (HprAD) transfected with small interfering siRNA targeting BBS1, BBS2 or BBS10, or a scrambled

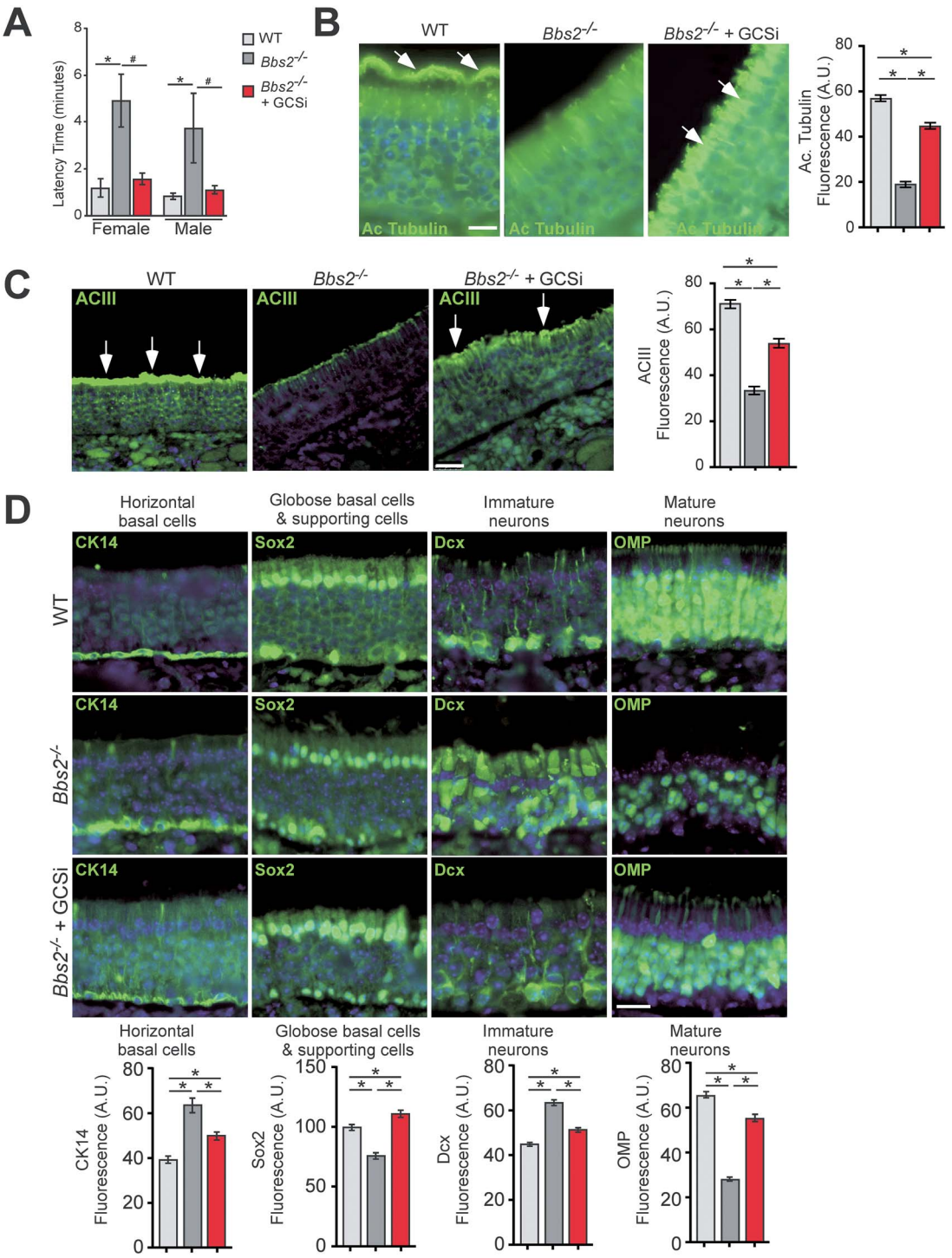

Figure 3. Genz-667161 treatment preserves cilia and preserves olfaction in *Bbs2*$^{-/-}$ mice. (**A**) Defects in olfaction were monitored *in vivo* using the buried treat test to measure the latency time to uncover a treat hidden beneath a layer of cage bedding (* indicates $P < 0.05$ WT versus *Bbs2*$^{-/-}$, # indicates $P < 0.05$ *Bbs2*$^{-/-}$ versus *Bbs2*$^{-/-}$ + GCSi). (**B**) Markers of cilia (acetylated tubulin, Ac. tubulin) and (**C**) odorant signaling (ACIII) was analyzed in nasal cavity sections of 6-month-old WT and *Bbs2*$^{-/-}$ mice, and *Bbs2*$^{-/-}$ littermates treated with GCSi along IF quantitation (* indicates $P < 0.05$). (**D**) Markers of cellular layers of the main olfactory epithelium were analyzed in the nasal cavity sections of WT and *Bbs2*$^{-/-}$ mice, and *Bbs2*$^{-/-}$ littermates treated with GCSi. Panels (from left to right) represent analysis of the horizontal basal cells stained with cytokeratin 14 (CK14), globose basal cells and supporting cells stained with SRY-Box 2 (Sox2), immature neurons stained with doublecortin (Dcx) and mature neurons stained olfactory marker protein (OMP) along IF quantitation below (* indicates $P < 0.05$). Error bars indicate SEM. Scale bar: 25 μm.

control with no known homology to human mRNAs. Analysis of gene expression by RT-qPCR demonstrated siRNA-specific suppression of *BBS1*, *BBS2* or *BBS10* transcripts (Fig. 6A). Enzyme-linked immunosorbent assay (ELISA) and Oil Red O staining revealed that *BBS1*, *BBS2* and *BBS10* knockdown increased leptin secretion and intracellular lipid accumulation, respectively, (Fig. 6B and C). In agreement with the observations in *Bbs2*$^{-/-}$ mice, Genz-667161 reduced leptin levels and lipid accumulation

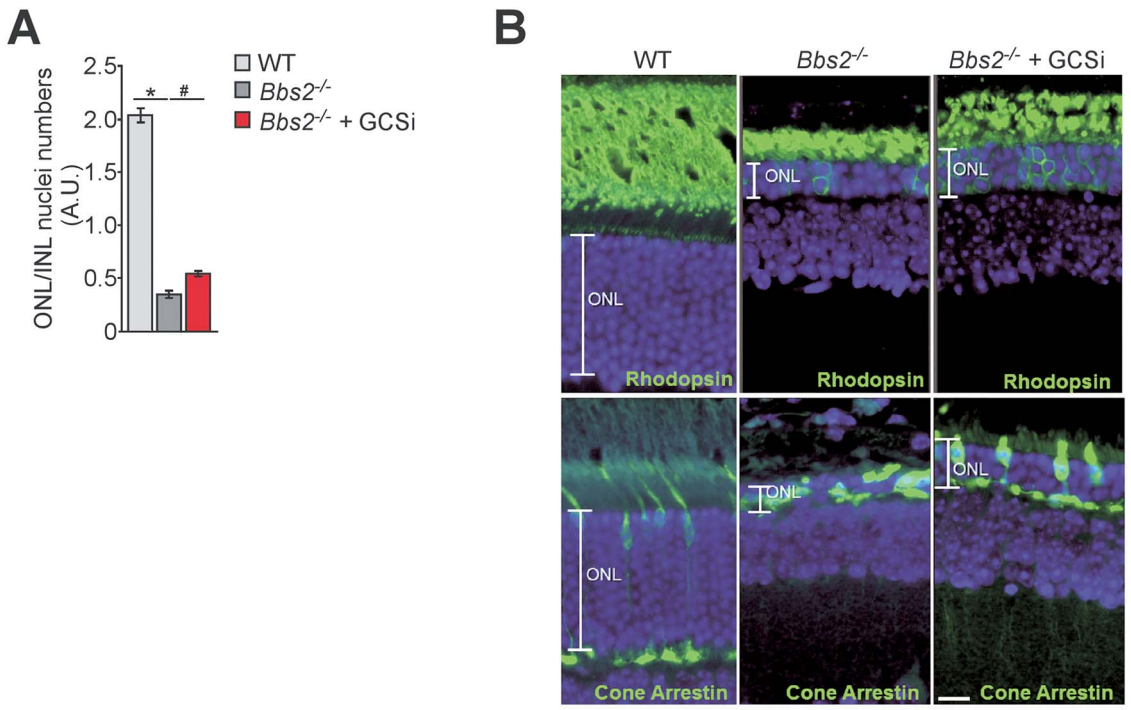

Figure 4. Genz-667161 delays retinal degeneration in *Bbs2*$^{-/-}$ mice. **(A)** Effect of GCSi on retinal thickness in 6-month-old *Bbs2*$^{-/-}$ mice, shown as the ratio of the number of nuclei per one vertical row in the outer nuclear layer (ONL) over inner nuclear layer (INL). **(B)** Analysis of the expression of rhodopsin (top) and cone arrestin (bottom) specific for rods and cones, respectively. Markers of retinal architecture were analyzed in eye sections of WT and *Bbs2*$^{-/-}$ mice, and *Bbs2*$^{-/-}$ littermates treated with GCSi. * indicates $P < 0.05$ WT versus *Bbs2*$^{-/-}$, # indicates $P < 0.05$ *Bbs2*$^{-/-}$ versus *Bbs2*$^{-/-}$ + GCSi; error bars indicate SEM. Scale bar: 25 µm.

in a dose-dependent fashion, adding credence to the notion that GCS inhibition can prevent the defect in adipocyte function that contributes to BBS (Fig. 6B and C).

Discussion

The findings described here provide compelling evidence that preservation of cilia structure and function through pharmacologic modulation of GSL metabolism is a viable approach for the treatment of multiple organ pathologies of BBS. Specifically, orally available brain-penetrant GlcCer Synthase inhibitor Genz-667161 administered to *Bbs2*$^{-/-}$ mice was effective in reducing obesity and liver weight as well as attenuated anosmia and retinal degeneration. Mechanistic studies confirmed that GM3 localization to the ciliary membrane must be tightly regulated to preserve ciliary structure and function, and suggest that Genz-667161 acts at least in part, by normalizing GM3 localization in the primary cilium (21).

We report for the first time that *Bbs2*$^{-/-}$ mice multi-organ pathology is associated with accumulation of GSLs. GlcCer is the first GSL in the GSL synthetic pathway synthesized by GCS, which catalyzes the transfer of glucose from UDP glucose to ceramide. We detected elevated levels of GlcCer in the serum, brain and peripheral tissues such as liver and kidney of *Bbs2*$^{-/-}$ mice. These findings are consistent with the increased GlcCer levels reported in murine models of obesity and suggest that abnormal GSL metabolism plays a key role in pathological weight gain irrespective of genetic lesion or endocrine defect (33).

We show that Genz-667161 administration to *Bbs2*$^{-/-}$ mice reduces circulating leptin levels, thereby decreased the hyperphagia and obesity that characterize this model. The role of BBS proteins in energy balance and satiety, which are regulated by leptin signaling in the hypothalamus, is well established (24,25,34–37). Our results indicate that GCS inhibition in *Bbs2*$^{-/-}$ mice leads to reduced food consumption by targeting the hypothalamic ciliary defect. These findings are consistent with the key role of hypothalamic ciliary signaling in the regulation of satiety. More specifically, BBS mice have decreased hypothalamic expression of proopiomelanocortin, whereas BBS1 regulates trafficking of the leptin receptor to the ciliary membrane (27,35). Moreover, cilia shortening in the hypothalamus of adult obese leptin-deficient mice leads to increased food intake and decreased energy expenditure (38).

Primary cilia and BBS proteins are necessary for adipocyte differentiation, suggesting that abnormal adipogenesis may contribute to the obesity phenotype of BBS. Indeed, pharmacological inhibition of GCS improved adipocyte function, insulin sensitivity, glucose homeostasis, and reduced inflammation in mouse models of diabetes or obesity (33,39–42). *In vitro* suppression of *BBS4*, *BBS10* and *BBS12* in differentiating preadipocytes promotes adipogenesis and fat accumulation (43,44). Obesity in BBS is believed to be secondary to adipocyte hyperplasia and hypertrophy (24). Inhibition of GCS prevents adipocyte hypertrophy thereby normalizing the adipocyte phenotype. Adipose tissue dysfunction is observed in non-alcoholic hepatic steatosis (45). Similarly, the liver phenotype in BBS patients is associated with obesity and overlaps with the manifestations of non-alcoholic fatty liver disease (28). *Bbs2*$^{-/-}$ mice showed elevated levels of serum triglycerides, ALT and increased liver weight, which were reduced by GCS inhibition.

RNA Seq analyses demonstrated that the loss of *Bbs2* caused changes in gene expression and that GCSi normalizes their expression closer to WT levels as shown by PCA. Canonical pathways involved in immune responses and genes involved

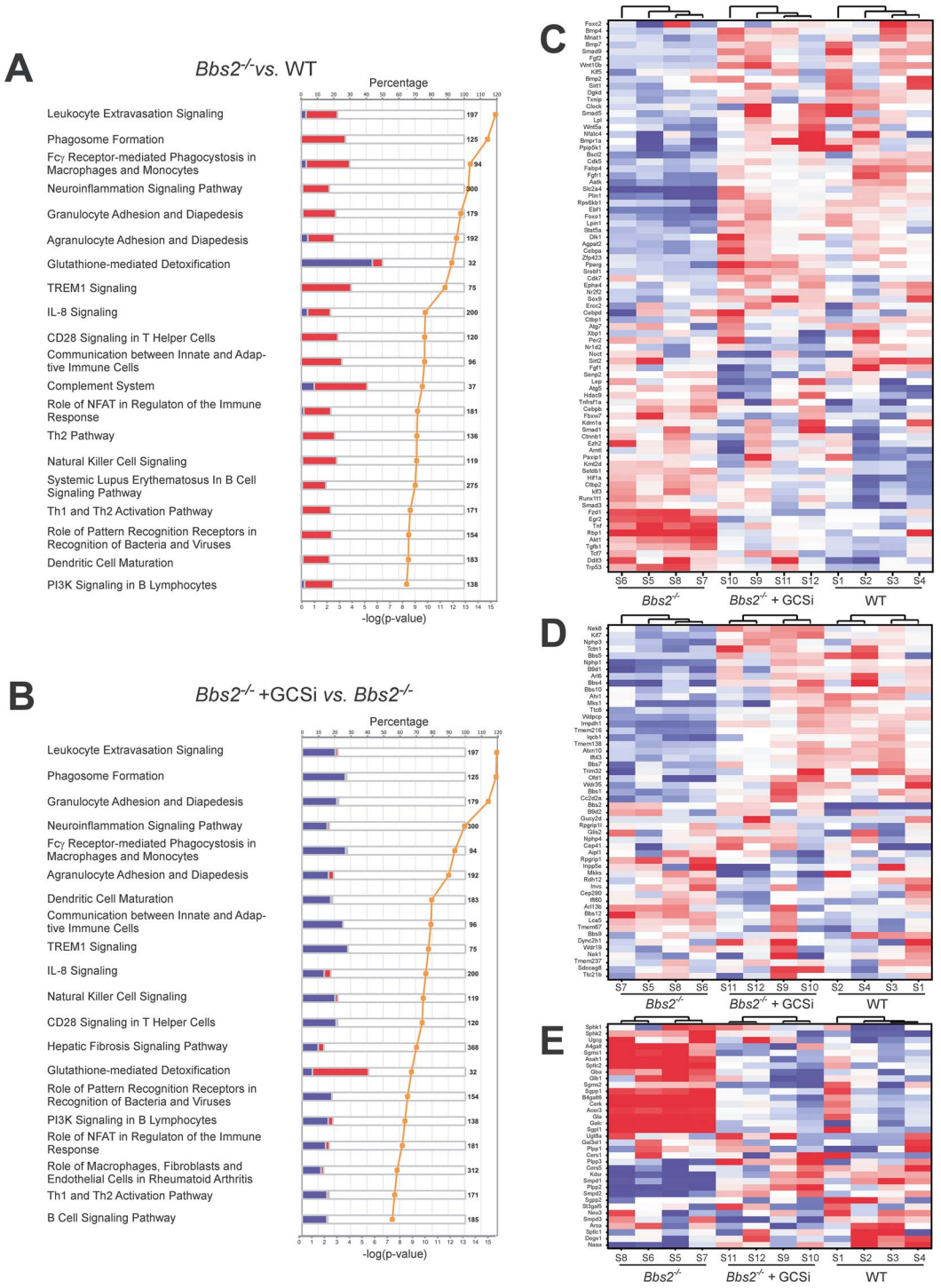

Figure 5. Transcriptomic changes in adipose tissue from WT, *Bbs2*$^{-/-}$ and *Bbs2*$^{-/-}$ + GCSi mice. **(A and B)** Twenty most altered canonical pathways between *Bbs2*$^{-/-}$ and WT mice (A) or *Bbs2*$^{-/-}$ mice and *Bbs2*$^{-/-}$ littermates treated with GCSi (B) adipose tissues from 6-month-old mice ($N = 4$ per group) along with *P*-values. **(C–E)** Heat map analyses of mRNA expressed in adipogenesis (C), ciliogenesis (D) and SL (E) pathways between WT (S1–4) and *Bbs2*$^{-/-}$ (S5–8) mice and *Bbs2*$^{-/-}$ littermates treated with GCSi (S9–12). Blue indicates low expression, and red indicates high expression. Raw values are presented in Supplementary Material, Tables 8–10, respectively.

in the biosynthesis of structural GSLs and signaling SLs, adipogenesis and ciliogenesis are dysregulated in adipose tissue of *Bbs2*$^{-/-}$ mice. GCS inhibition normalized their expression. Indeed, an increase in *Ugcg* mRNA coding for GCS is observed in *Bbs2*$^{-/-}$ mice and its expression is downregulated by GCSi, suggesting that the reduction of GlcCer observed could be the result of both the inhibition of GCS and of the reduction of GCS enzyme. These data are correlated with the demonstrated role of GlcCer in the differentiation of mesenchymal stem cells into adipocytes in white adipose tissue in mice and in the control of energy metabolism in Drosophila (46,47). Similarly, an increase in the mRNA B4galt6 coding for the enzyme galactosyltransferase

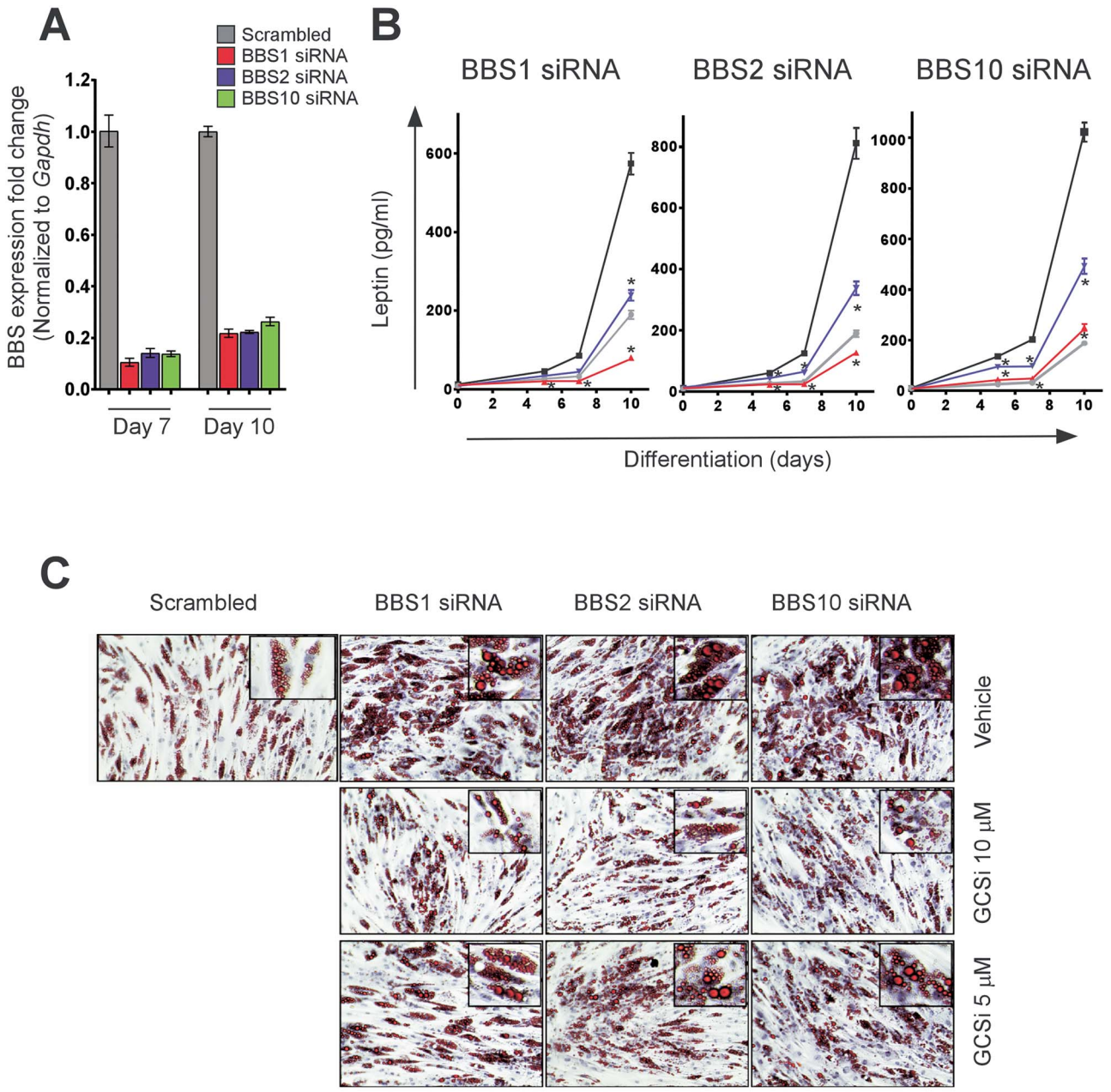

Figure 6. Genz-667161 reduces BBS1-, 2- or 10-dependent adipogenesis and leptin secretion in HprAD *in vitro*. (**A**) RT-qPCR quantitation of BBS1, 2 or 10 upon knockdown with specific siRNA as expressed as fold change over scrambled siRNA controls in HprAD normalized to GAPDH. (**B**) Effect of GCSi on leptin secretion upon BBS1, 2 or 10 knockdown in HprAD cells. Cell culture media were harvested at days 0, 5, 7 and 10, and leptin was quantified by ELISA. Data are represented as mean leptin concentrations ± SEM for scrambled controls siRNA (gray •) and BBS siRNAs as noted in figure, in vehicle (black ■), GCSi 5 μM (blue ▼) or GCSi 10 μM (red ▲). *$P < 0.05$ compared to vehicle. (**C**) Effect of GCSi on BBS1, 2 or 10 knockdown in HprAD cells on lipid accumulation. Photon micrograph of representative field of HprAD cells stained with Oil Red O. Data are representative of three independent experiments.

responsible for the formation of lactosylceramide (LacCer) is observed in *Bbs2*$^{-/-}$ mice. Immune responses may require LacCer, a constituent of certain cell membrane microdomains that is involved in immune response by playing a role in the secretion of cytokines such as tumor necrosis factor-alpha (TNFα), which has also been found to be upregulated in *Bbs2*$^{-/-}$ mice adipose tissue and downregulated by GCSi (48). It is plausible that TNFα is directly secreted by adipocytes, although other cells types present in adipose tissue, including preadipocytes, endothelial cells, smooth muscle cells, fibroblasts, leukocytes and macrophages, may produce more TNFα than adipocytes (49). Increases in mRNA encoding for enzymes involved in GSL signaling are also observed in adipose tissue of *Bbs2*$^{-/-}$ mice and normalized by Genz-667161. These include sphingosine kinases 1/2 mRNA (Sphk1/2). Sphingosine-1 phosphate (S1P), the product of Sphk1/2 seems to promote macrophages survival in adipose tissue that may contribute to increase inflammation (50).

Ciliogenesis initiates in the G1 phase of the cell cycle and progresses as cells move through the G1 and enter the G0 phase. Assembly requires the coordinated delivery of proteins to the

ciliary base by multiple trafficking pathways, and presence of the BBSome, a multimolecular complex of highly specialized proteins (11). Many genes critical for cilia assembly, maintenance or function of full-length cilia (including vesicle trafficking, transition zone and intraflagellar transport complex components) are decreased in *Bbs2*$^{-/-}$ mice. This is consistent with defective ciliogenesis and cell cycle progression, as cilium formation and resorption is tightly controlled during the cell cycle. Treatment of *Bbs2*$^{-/-}$ mice with a GCSi not only reduces the expression level of ciliary genes to near WT levels, but also increases ciliary length and reduces GM3 accumulation. It is plausible that GCSi treatment normalizes cell cycle progression towards a WT phenotype by reducing GM3 levels. This would allow ciliary assembly to resume, maintaining cilia length and function and lessening the impact of the *BBS2* mutation.

We show that the olfactory response of *Bbs2*$^{-/-}$ mice was improved by GCSi treatment, and this effect correlated with a preservation of the cilia morphology and signaling in the olfactory epithelium. In the MOE, olfactory sensory neurons (OSN) express ciliary receptors that initiate the olfactory response. Upon odorant contact and receptor activation, olfaction signaling is initiated through activation of ACIII (51,52). Similar to findings in *Bbs1*, *Bbs4* and *Bbs8* null mice, *Bbs2* deletion decreases ACIII at the MOE, and this effect is improved by GCSi treatment (29,53). *Bbs2*$^{-/-}$ mice show a decreased number of mature neurons in the MOE that was reversed upon GCS inhibition. This observation suggests that the beneficial effects of GCS inhibition on the MOE are mediated by the preservation of cilia and maintenance of ciliary-related odorant signaling and neuronal differentiation.

Retinal degeneration in BBS patients is particularly devastating, progressing rapidly and causing legal blindness by the age of 20 (54). In the photoreceptor cells, the connecting cilium is the only structure integrating the inner and outer segments. Mutations in BBS genes likely compromise trafficking of proteins from the inner segment through the connecting cilium to the outer segment (51). Mouse models of BBS recapitulate the retinal degeneration that is evident in the human disease and suggest that mislocalization of rhodopsin may contribute to vision loss (16,55–59). The onset of retinal degeneration in *Bbs2*$^{-/-}$ mice is very rapid, with a significant degree of retinal ONL degeneration of the ONL leading to a major decline in photoreceptor function by 10 weeks of age. Photoreceptor cell death was preceded by mislocalization of rhodopsin, confirming the defect in protein transport (16). Remarkably, administration of Genz-667161 to *Bbs2*$^{-/-}$ mice had a positive effect on retinal degeneration by increasing the thickness of the ONL. Also, treatment partially corrected the localization of rhodopsin and cone arrestin, corroborating the ability of GCSi to modulate protein transport.

Therapies addressing specific facets of BBS pathology are beginning to emerge. For example, melanocortin receptor agonists are being tested in preclinical and clinical trials as potential treatment for the obesity; however, they are not expected to address other disease manifestations (54,60). The development of new therapeutic approaches to address multi-tissue pathogenesis of BBS ciliopathies is urgently needed. Our data show that genetic reduction of BBS1, BBS2 or BBS10 in human preadipocytes increases lipid accumulation and leptin secretion reminiscent of previous studies (43,44). GCS inhibition in this study reduced lipid accumulation and leptin secretion, suggesting that GCSi treatment could be beneficial to BBS2 patients as well as to BBS patients harboring BBS1 or BBS10 mutations. Treatment of these three groups would encompass ~50% of all BBS patients (31).

Gene therapy efforts to target olfaction or retinal defects in BBS mice have been described. Studies conducted in *Bbs1* mutant mice showed that adeno-associated virus (AAV)-mediated delivery of WT *Bbs1* restored OSN cilia, corrected BBSome cilium trafficking defects and restored olfactory response (61). However, the 60–90-day turnover of OSN, combined with the fact that the host immune response prevents multiple AAV administrations, limits this approach. Moreover, intranasal delivery only reaches cells exposed to the apical surface of the olfactory epithelium and not the underlying immature neurons (62).

Several studies demonstrated that gene therapy prevents photoreceptor death and preserves retinal function (54,63,64). AAV-mediated *Bbs4* delivery into the rods of *Bbs4* mutant mice rescued the rhodopsin mislocalization and restored rod morphology. Treatment also prevented photoreceptor death and improved electrophysiological function (63). AAV delivery of *Bbs1* into *Bbs1*-null mice rescued BBSome formation, rhodopsin localization and lead to a trend toward a functional improvement (54). This study highlighted some challenges associated with a gene therapy approach, as the treatment damaged the ONL in the retina at the site of the injection bleb. Toxicity could be due to overexpression of the BBS1 protein or a disruption of the BBSome stoichiometry (54). The fact that there was no associated toxicity with overexpression of BBS1 in the OSN may reflect a different tolerance of distinct tissues to overexpression. The main challenge of a gene therapy approach is the heterogeneity of BBS mutations. This would require correction of each individual genetic defect so that dosage and toxicity would have to be established for each gene-specific therapeutic. Also, a gene therapy approach is unlikely to address the multi-organ pathophysiology in BBS. Therefore, we propose that the pharmacological restoration of cilia structure and function is a unique opportunity to address the multiple manifestations of BBS regardless of genetic lesion.

In conclusion, our data demonstrate for the first time that GSL metabolism is dysregulated in BBS. This metabolic defect can be targeted by GCS inhibition to maintain cilia structure and signaling, resulting in improvement of pathology in multiple organs. Taken together, our data suggest that this therapeutic approach will be beneficial to multiple ciliopathies irrespective of the underlying mutation.

Materials and Methods

Generation of a mouse model of BBS2

To generate a mouse model of BBS2, we sought to delete exons 5–13 of the *Bbs2* locus. To this end, a targeting vector containing a *LacZ-lox*^{P}*-Ub1-em7-Neo-lox*^{P} (Neo) cassette (2648 bp) flanked by 5′ and 3′ homology arms complementary to intron 4 and intron 13 of the *Bbs2* gene, respectively, was designed commercially (Regeneron, Tarrytown, NY). The construct was engineered to delete 13 020 base pairs (bp) of the targeted region (chr8:96599337-96612356) and replace with the Neo cassette. Subsequently, C57BL/6F1 embryonic stem cells were electroporated with the linearized targeting vector, and resulting positive clones were microinjected into 8-cell stage mouse C57BL/6 embryos using Regeneron's VelociMouse® platform (65). The embryos were then transferred to uteri of pseudo-pregnant recipient females. Weaned pups were scored, and high-percentage chimera males were selected for mating with C57BL/6 female mice expressing Cre-recombinase under the control of a ubiquitously expressed promoter to remove the neo cassette. PCR-screening and sequence validation confirmed two

positive clones for the desired mutation. A mutant founder was selected for expansion and production of study cohorts.

WT and knockout (KO) animals were identified by genomic tail DNA probed with PCR applying the following primer pairs: KO-Forward: 5′ TGC CAA GGG GTT TTG TAG G 3′, KO-Reverse: 5′ GCC ATG CAT ATA ACT TCG TAT AGC 3′, KO-Probe: 5′ AGC AGT TTT CAG GTG ACC CTG CTT TC 3′, WT-Forward: 5′ T TGT CCT GAA GCT GCA TAG CC 3′, WT-Reverse: 5′ GAC TGA GAG CGC TGT GTG G 3′, WT-Probe: 5′ CAG AAA GGC ATA ATC CCA 3′, yielding a 95 and 184 bp-product, respectively.

Breeding, general husbandry and Genz-667161 administration

To generate two different incipient congenic strains, heterozygous *Bbs2*$^{-/+}$ mice on a C57BL/6 genetic background were backcrossed into a 129S6/SvEv inbred background by using speed congenic program to accelerate generational breeding. Mice were maintained in a mixed C57BL/6;129S6/SvEv background at Jackson Laboratories (Bar Harbor) under specific pathogen-free conditions. All mouse experiments were approved by the Institutional Animal Care and Use Committees of the Jackson Laboratories and Sanofi.

To verify *Bbs2* mRNA KO, adipose tissue was extracted as described in section RNA extraction, RNAseq library construction and data analysis below and RT-qPCR was performed with Taqman primer and probe set spanning exon 12–13 (Cat# Mm00518141_m1) or spanning exon 16–17 (Cat# Mm01249575_m1) and normalized with 18 s primer set (Cat# Mm01249575_m1) as recommended by the manufacturer (LifeTechnologies).

Genz-667161 (quinuclidin-3-yl N-[1-[3-(4-fluorophenyl)phenyl]-1-methyl-ethyl]carbamate), a brain-penetrant GCSi, was administered ad libitum to several cohorts of *Bbs2*$^{-/-}$ mice by mixing in pelleted 5053 diet (LabDiet) at 0.033% (weight/weight) from 1 to 6 months of age in >2 studies with similar outcomes (66). Tissues were harvested for histological analysis at 6 months of age and fixed in 4% paraformaldehyde (Electron Microscopy Science) or flash frozen and stored at −80°C for gene expression analyses. Triglyceride and ALT levels were measured using a VetAce™ analyzer (Alfa Wassermann) in 6-month-old animals.

GSL analysis

Quantitative analysis of SLs was performed by liquid chromatography and high-resolution or tandem mass spectrometry (LC/HR-MS or LC/MS/MS). Tissue homogenization, GlcCer and PC extractions, and analyses were performed as previously described with modifications for GM3 analysis as follows (67). Briefly, 10 µL of tissue homogenate (liver, brain or kidney) or 10 µL of serum were extracted with a solvent consisting of equal volume of acetonitrile and methanol. GM3 was separated with isocratic elution using a mobile phase consisting of acetonitrile:methanol:water (61.75:33.23:5 vol/vol) in 10 mM of ammonium acetate, pH 6.8 for 2 min using a Waters Acquity UPLC and Waters Atlantis HILIC Silica column (3 µm, 2.1 × 100 mm) at room temperature. The flow rate was 0.4 mL/min. The eluent was analyzed by a Q Exactive mass spectrometer (ThermoFisher Scientific) equipped with a Heated ElectroSpray Ionization source. Data were collected in full MS negative mode using the following parameters: resolution of 70 000, scan range of 1100–1700 m/z, AGC target of 3e6, and max IT of 256 ms. Quantitation of different isoforms with various acyl chain lengths was achieved by MS1 extraction of ion chromatograms. GM3 standard was purchased from Matreya, LLC.

Histological analysis

H&E-stained slides were scanned at a 20X magnification using the Aperio ScanScope XT (Leica Biosystems). Images were evaluated for quality using the Aperio eSlide Manager Viewer (Leica Biosystems). Automated digital image analysis was performed on whole adipose tissues using the Visiopharm Image Analysis software (DK-2970 Hoersholm, Denmark, version 6.9.1). Two custom-written applications were created and run consecutively for each digital image. The first application detected adipose tissue using threshold classification and outlined the area as a region of interest (ROI). The second application used threshold to classify the tissue inside the ROI into three categories: cytoplasm (cytoplasmic membrane), adipose (adipocyte) and other (unwanted artifacts, large vessels, other tissues). Post-processing steps included enclosing adipose with cytoplasm and selecting adequate adipose cells for counting by removing any adipose with a form factor less than 0.5. Selected adipose were then classified according to size (small: $1000 \leq 4000$ µm^2, medium: $4000 \leq 7000$ µm^2, large: $7000 \leq 25\,000$ µm^2). The results are reported as % adipose by size.

Metabolic analysis

Whole body fat and lean mass were measured monthly from 3 months of age until 6 months of age by nuclear magnetic resonance imaging (EchoMRI™ mouse, Echo Medical Systems). Percentage body fat was calculated using the following formula: (fat mass/(fat mass + lean mass)) × 100. Average food consumption per animal per day was estimated from 5.5 to 6 months of age using the following formula: [(food weight at start of period-(food weight at end of period in hopper + food weight at end of period in bedding)]/number of animals in the cage/number of days of observation. Body weight was recorded for individual animals at time points indicated in results.

Olfaction analysis

Animal olfaction was tested at 6 months of age in accordance to Yang *et al.* (68), with modifications. Before testing, animals were acclimated for 3 days and then fasted for 18 h in a cage with Alpha Dri bedding. A Supreme Mini-Treats™, Chocolate flavor treat (BioServ) was buried 1 cm deep in a clean cage with 3-cm-deep bedding. Animals were placed in the clean cage, and the latency time to find treat was recorded. If the subject failed to find the treat after 10 min had elapsed, the test was stopped and a 10 min long latency score was recorded.

Cell culture

Immortalized WT and *Bbs2*$^{-/-}$ kidney epithelium cell lines were established from WT and *Bbs2*$^{-/-}$ kidney and maintained as described previously (69,70). For cilia analysis, cells were cultured on collagen type-I-coated glass slides in complete culture medium followed by an additional 24 h in serum-free medium. To study the role of GCS inhibition, cells were cultured for 48 h on collagen type-I-coated glass slides in complete medium and 24 h in serum-free medium followed by 24 h in serum-free medium containing 5 µM Genz-667161. Cilia length was measured in cultured cells using Metamorph Imaging Series® Software after staining with acetylated tubulin.

In vitro adipocyte differentiation

HprAD (Lonza Cat# PT-5001) were plated PGM-2 Preadipocyte Growth Medium-2 BulletKit, (Lonza) at 30 000 cells/cm^2 density and grown at 37°C overnight. The next day, cells were transfected with scrambled or BBS1-, BBS2-, BBS10-specific siRNA in OptiMem (Invitrogen) using Lipofectamine 2000 (Invitrogen) and RDM-2 medium (Lonza) is added to allow differentiation to proceed for 10 days with ethanol (vehicle) or in the presence of 5 or 10 μM Genz-667161 as stated in the figure legend. Photon microscopy (Axiovert 25, Zeiss) was used to appreciate lipid accumulation, which is evident by the size and quantity of red lipid vacuoles in the cells upon Oil Red O staining (Biovision). In parallel, a set of knockdown experiments were performed to measure the levels of BBS1, BBS2 and BBS10 mRNA upon respective knockdowns by RT-qPCR and harvested at day 7 and 10 post knockdown. RNA was harvested using cell to Ct kit as recommended by the manufacturer (Applied Biosystems) and levels of *BBS1*, *BBS2* or *BBSbs*10 mRNA were determined with specific Taqman assays (Applied Biosystems).

Leptin analysis

Serum samples were obtained by heart puncture from 6-month-old WT, *Bbs2*$^{-/-}$ and *Bbs2*$^{-/-}$ mice treated with GCSi or from cell culture supernatants after 0, 5, 7 and 10 days of adipocytes differentiation. Serum and cell culture supernatant leptin concentrations were measured by ELISA according to the manufacturer's instructions (R&D Systems).

RNA extraction, RNAseq library construction and data analysis

RNA was isolated by TRIzol and chloroform extraction from homogenized adipose tissue dissected from four 6-month-old WT, *Bbs2*$^{-/-}$ and *Bbs2*$^{-/-}$ GCSi-treated mice, followed by RNeasy purification to remove genomic DNA (Qiagen). RNA purity was assessed using a Nanodrop 800 system, and RNA integrity was evaluated using the Agilent 2200 Tape Station (Agilent Technologies). The sequencing libraries were generated using the TruSeq Stranded mRNA Library Prep Kit as per the manufacturer recommendations (Illumina). Sequencing was performed using High Output NextSeq 500/550 v2.5 kits on an Illumina NextSeq 500 platform (2 × 75-bp paired-end reads).

Data analysis was performed with Array Studio V10.1 (Omicsoft Corporation, a Qiagen company) and mapped to Genome Reference Consortium Mouse Build 38. Differentially expressed genes were chosen according to the criteria of fold change >2.0 and adjusted *P*-value <0.05. All the differentially expressed genes were used for ingenuity pathway analysis (IPA- https://www.qiagenbioinformatics.com/products/ingenuity-pathway-analysis according to algorithms previously described (71)). Heatmaps were generated using a center scale normalization algorithm on median normalized Log 2 expression values as per the software developer (Omicsoft). Data are available from the Gene Expression Omnibus with submission number GSE149866 (https://www.ncbi.nlm.nih.gov/geo/query/acc.cgi?acc=GSE149866).

IF analysis

IF was performed on paraformaldehyde-fixed paraffin-embedded sections as previously described (72). Briefly, sections were deparaffinized, subjected to antigen retrieval and incubated overnight with primary antibodies at 4°C. Primary antibodies to ACIII (Santa Cruz Biotechnology), acetylated tubulin, SRY-Box 2 and Dcx (Cell Signaling Technology), rhodopsin (Thermo Scientific), cone arrestin (EMD Millipore), CK14 (Protein Tech) and OMP (Wako) were incubated overnight at 4°C. Primary antibodies were revealed with Alexa Fluor 488-conjugated secondary antibodies (Thermo Scientific). IF quantitation was performed using ImageJ software (National Institute of Health), and statistical analyzes were performed as described below.

For IF analysis of cultured cells, samples were fixed with 4% paraformaldehyde followed by staining with antibodies against GM3 (Creative Biolabs) and acetylated tubulin followed by Alexa Fluor 488- or Alexa Fluor 594-conjugated secondary antibodies, as previously described (73). Images were acquired on a Leica DM5500B microscope fitted with ×40 and ×60 objectives using Leica Application Suite Advance Fluorescence software (Leica Microsystems). Cilia length was quantified with the MetaMorph Imaging Series® software (Molecular Devices LLC).

Statistical analysis

Results were expressed as means ± standard error of the mean (SEM). All analyses were performed using Statistical Analysis System (SAS 9.4) software in Everst@t version 6.1 software. Normality test followed by Levene test for equal variances was performed. While the distributions were normal, based on the determination that the variances are significantly different ($P < 0.0001$), the non-parametric Kruskal–Wallis test followed by Wilcoxon pairwise comparisons was used to compare groups. Significance was accepted at the 0.05 level of probability.

Author Contributions

N.O.B., S.M. and H.H. designed and conducted experiments, analyzed data and wrote the manuscript. O.B. designed experiments, analyzed the data, wrote the manuscript with contributions from N.O.B., S.M., T.P. and H.H. and supervised the project. M.M.S. performed *in vivo* and *in vitro* work and data analysis. H.P. and B.W. carried out GSL analysis. N.O.B., R.J.R. and H.H. performed image processing and histological quantification. B.R., C.Z. and S.L.M. performed and analyzed RNAseq data. T.A.N., V.M., T.P., L.A.S., S.L.M., C.Z., K.W.K and S.Z. provided scientific advice, analyzed data and edited the manuscript.

Supplementary Material

Supplementary material is available at *HMG* online.

Acknowledgements

We thank the staff of the Sanofi In Vivo Research Center and Histology Departments for help with *in vivo* studies and sample preparation, as well as Cynthia Pryce and William Weber for quantitative analysis of adipose tissue. We are grateful to Dr Seng Cheng for helpful discussions and comments on this manuscript, to Dr Catherine O'Riordan for her helpful advice on the study of retinal degeneration and to Dr Mostafa Kabiri for the generation of the *Bbs2*$^{-/-}$ mice. This work was supported by Sanofi.

Conflict of Interest statement. All authors were employed by Sanofi at the time experiments were executed.

References

1. Waters, A.M. and Beales, P.L. (2011) Ciliopathies: an expanding disease spectrum. *Pediatr. Nephrol.*, **26**, 1039–1056.
2. Reiter, J.F. and Leroux, M.R. (2017) Genes and molecular pathways underpinning ciliopathies. *Nat. Rev. Mol. Cell Biol.*, **18**, 533–547.
3. Mitchison, H.M. and Valente, E.M. (2017) Motile and non-motile cilia in human pathology: from function to phenotypes. *J. Pathol.*, **241**, 294–309.
4. Lee, J.E. and Gleeson, J.G. (2011) A systems-biology approach to understanding the ciliopathy disorders. *Genome Med.*, **3**, 59.
5. Khan, S.A., Muhammad, N., Khan, M.A., Kamal, A., Rehman, Z.U. and Khan, S. (2016) Genetics of human Bardet-Biedl syndrome, an updates. *Clin. Genet.*, **90**, 3–15.
6. Heon, E., Kim, G., Qin, S., Garrison, J.E., Tavares, E., Vincent, A., Nuangchamnong, N., Scott, C.A., Slusarski, D.C. and Sheffield, V.C. (2016) Mutations in C8ORF37 cause Bardet Biedl syndrome (BBS21). *Hum. Mol. Genet.*, **25**, 2283–2294.
7. Schaefer, E., Stoetzel, C., Scheidecker, S., Geoffroy, V., Prasad, M.K., Redin, C., Missotte, I., Lacombe, D., Mandel, J.L., Muller, J. *et al.* (2016) Identification of a novel mutation confirms the implication of IFT172 (BBS20) in Bardet-Biedl syndrome. *J. Hum. Genet.*, **61**, 447–450.
8. Novas, R., Cardenas-Rodriguez, M., Irigoin, F. and Badano, J.L. (2015) Bardet-Biedl syndrome: is it only cilia dysfunction? *FEBS Lett.*, **589**, 3479–3491.
9. Zhang, Q., Yu, D., Seo, S., Stone, E.M. and Sheffield, V.C. (2012) Intrinsic protein-protein interaction-mediated and chaperonin-assisted sequential assembly of stable bardet-biedl syndrome protein complex, the BBSome. *J. Biol. Chem.*, **287**, 20625–20635.
10. Haws, R.M., Krentz, A.D., Stankowski, R.V. and Steiner, R.D. (2015) Bardet-Biedl syndrome: a model for translational research in rare diseases. *New Horiz. Trans. Med.*, **2**, 102–109.
11. Nachury, M.V., Loktev, A.V., Zhang, Q., Westlake, C.J., Peranen, J., Merdes, A., Slusarski, D.C., Scheller, R.H., Bazan, J.F., Sheffield, V.C. *et al.* (2007) A core complex of BBS proteins cooperates with the GTPase Rab8 to promote ciliary membrane biogenesis. *Cell*, **129**, 1201–1213.
12. Loktev, A.V., Zhang, Q., Beck, J.S., Searby, C.C., Scheetz, T.E., Bazan, J.F., Slusarski, D.C., Sheffield, V.C., Jackson, P.K. and Nachury, M.V. (2008) A BBSome subunit links ciliogenesis, microtubule stability, and acetylation. *Dev. Cell*, **15**, 854–865.
13. Seo, S., Baye, L.M., Schulz, N.P., Beck, J.S., Zhang, Q., Slusarski, D.C. and Sheffield, V.C. (2010) BBS6, BBS10, and BBS12 form a complex with CCT/TRiC family chaperonins and mediate BBSome assembly. *Proc. Natl. Acad. Sci. USA.*, **107**, 1488–1493.
14. Jin, H., White, S.R., Shida, T., Schulz, S., Aguiar, M., Gygi, S.P., Bazan, J.F. and Nachury, M.V. (2010) The conserved Bardet-Biedl syndrome proteins assemble a coat that traffics membrane proteins to cilia. *Cell*, **141**, 1208–1219.
15. Norris, D.P. and Grimes, D.T. (2012) Mouse models of ciliopathies: the state of the art. *Dis. Models Mech.*, **5**, 299–312.
16. Nishimura, D.Y., Fath, M., Mullins, R.F., Searby, C., Andrews, M., Davis, R., Andorf, J.L., Mykytyn, K., Swiderski, R.E., Yang, B. *et al.* (2004) Bbs2-null mice have neurosensory deficits, a defect in social dominance, and retinopathy associated with mislocalization of rhodopsin. *Proc. Natl. Acad. Sci. USA.*, **101**, 16588–16593.
17. Lahiri, S. and Futerman, A.H. (2007) The metabolism and function of sphingolipids and glycosphingolipids. *Cell. Mol. Life Sci.*, **64**, 2270–2284.
18. Chatterjee, S., Shi, W.Y., Wilson, P. and Mazumdar, A. (1996) Role of lactosylceramide and MAP kinase in the proliferation of proximal tubular cells in human polycystic kidney disease. *J. Lipid Res.*, **37**, 1334–1344.
19. Rani, C.S., Abe, A., Chang, Y., Rosenzweig, N., Saltiel, A.R., Radin, N.S. and Shayman, J.A. (1995) Cell cycle arrest induced by an inhibitor of glucosylceramide synthase. Correlation with cyclin-dependent kinases. *J. Biol. Chem.*, **270**, 2859–2867.
20. Zeidan, Y.H. and Hannun, Y.A. (2007) Translational aspects of sphingolipid metabolism. *Trends Mol. Med.*, **13**, 327–336.
21. Janich, P. and Corbeil, D. (2007) GM1 and GM3 gangliosides highlight distinct lipid microdomains within the apical domain of epithelial cells. *FEBS Lett.*, **581**, 1783–1787.
22. Wang, G., Krishnamurthy, K. and Bieberich, E. (2009) Regulation of primary cilia formation by ceramide. *J. Lipid Res.*, **50**, 2103–2110.
23. Kong, J.N., Hardin, K., Dinkins, M., Wang, G., He, Q., Mujadzic, T., Zhu, G., Bielawski, J., Spassieva, S. and Bieberich, E. (2015) Regulation of Chlamydomonas flagella and ependymal cell motile cilia by ceramide-mediated translocation of GSK3. *Mol. Biol. Cell*, **26**, 4451–4465.
24. Marion, V., Mockel, A., De Melo, C., Obringer, C., Claussmann, A., Simon, A., Messaddeq, N., Durand, M., Dupuis, L., Loeffler, J.P. *et al.* (2012) BBS-induced ciliary defect enhances adipogenesis, causing paradoxical higher-insulin sensitivity, glucose usage, and decreased inflammatory response. *Cell Metabol.*, **16**, 363–377.
25. Sherafat-Kazemzadeh, R., Ivey, L., Kahn, S.R., Sapp, J.C., Hicks, M.D., Kim, R.C., Krause, A.J., Shomaker, L.B., Biesecker, L.G., Han, J.C. *et al.* (2013) Hyperphagia among patients with Bardet-Biedl syndrome. *Pediatr. Obes.*, **8**, e64–e67.
26. Seo, S., Guo, D.F., Bugge, K., Morgan, D.A., Rahmouni, K. and Sheffield, V.C. (2009) Requirement of Bardet-Biedl syndrome proteins for leptin receptor signaling. *Hum. Mol. Genet.*, **18**, 1323–1331.
27. Guo, D.F., Cui, H., Zhang, Q., Morgan, D.A., Thedens, D.R., Nishimura, D., Grobe, J.L., Sheffield, V.C. and Rahmouni, K. (2016) The BBSome controls energy homeostasis by mediating the transport of the Leptin receptor to the plasma membrane. *PLoS Genet.*, **12**, e1005890.
28. Branfield Day, L., Quammie, C., Heon, E., Bhan, A., Batmanabane, V., Dai, T. and Kamath, B.M. (2016) Liver anomalies as a phenotype parameter of Bardet-Biedl syndrome. *Clin. Genet.*, **89**, 507–509.
29. Kulaga, H.M., Leitch, C.C., Eichers, E.R., Badano, J.L., Lesemann, A., Hoskins, B.E., Lupski, J.R., Beales, P.L., Reed, R.R. and Katsanis, N. (2004) Loss of BBS proteins causes anosmia in humans and defects in olfactory cilia structure and function in the mouse. *Nat. Genet.*, **36**, 994–998.
30. Tobin, J.L. and Beales, P.L. (2007) Bardet-Biedl syndrome: beyond the cilium. *Pediatr. Nephrol.*, **22**, 926–936.
31. M'Hamdi, O., Ouertani, I. and Chaabouni-Bouhamed, H. (2014) Update on the genetics of bardet-biedl syndrome. *Mol. Syndromol.*, **5**, 51–56.
32. Forsythe, E. and Beales, P.L. (2013) Bardet-Biedl syndrome. *Eur. J. Hum. Genet.*, **21**, 8–13.
33. Aerts, J.M., Ottenhoff, R., Powlson, A.S., Grefhorst, A., van Eijk, M., Dubbelhuis, P.F., Aten, J., Kuipers, F., Serlie, M.J., Wennekes, T. *et al.* (2007) Pharmacological inhibition of glucosylceramide synthase enhances insulin sensitivity. *Diabetes*, **56**, 1341–1349.
34. Lopez, M. (2016) Hypothalamic Leptin resistance: from BBB to BBSome. *PLoS Genet.*, **12**, e1005980.

35. Rahmouni, K., Fath, M.A., Seo, S., Thedens, D.R., Berry, C.J., Weiss, R., Nishimura, D.Y. and Sheffield, V.C. (2008) Leptin resistance contributes to obesity and hypertension in mouse models of Bardet-Biedl syndrome. *J. Clin. Invest.*, **118**, 1458–1467.
36. Feuillan, P.P., Ng, D., Han, J.C., Sapp, J.C., Wetsch, K., Spaulding, E., Zheng, Y.C., Caruso, R.C., Brooks, B.P., Johnston, J.J. *et al.* (2011) Patients with Bardet-Biedl syndrome have hyperleptinemia suggestive of leptin resistance. *J. Clin. Endocrinol. Metab.*, **96**, E528–E535.
37. Kwon, O., Kim, K.W. and Kim, M.S. (2016) Leptin signalling pathways in hypothalamic neurons. *Cell. Mol. Life Sci.*, **73**, 1457–1477.
38. Han, Y.M., Kang, G.M., Byun, K., Ko, H.W., Kim, J., Shin, M.S., Kim, H.K., Gil, S.Y., Yu, J.H., Lee, B. *et al.* (2014) Leptin-promoted cilia assembly is critical for normal energy balance. *J. Clin. Invest.*, **124**, 2193–2197.
39. Zhao, H., Przybylska, M., Wu, I.H., Zhang, J., Siegel, C., Komarnitsky, S., Yew, N.S. and Cheng, S.H. (2007) Inhibiting glycosphingolipid synthesis improves glycemic control and insulin sensitivity in animal models of type 2 diabetes. *Diabetes*, **56**, 1210–1218.
40. van Eijk, M., Aten, J., Bijl, N., Ottenhoff, R., van Roomen, C.P., Dubbelhuis, P.F., Seeman, I., Ghauharali-van der Vlugt, K., Overkleeft, H.S., Arbeeny, C. *et al.* (2009) Reducing glycosphingolipid content in adipose tissue of obese mice restores insulin sensitivity, adipogenesis and reduces inflammation. *PLoS One*, **4**, e4723.
41. Yew, N.S., Zhao, H., Hong, E.G., Wu, I.H., Przybylska, M., Siegel, C., Shayman, J.A., Arbeeny, C.M., Kim, J.K., Jiang, C. *et al.* (2010) Increased hepatic insulin action in diet-induced obese mice following inhibition of glucosylceramide synthase. *PLoS One*, **5**, e11239.
42. Furukawa, K., Ohmi, Y., Kondo, Y., Ohkawa, Y., Tajima, O. and Furukawa, K. (2015) Regulatory function of glycosphingolipids in the inflammation and degeneration. *Arch. Biochem. Biophys.*, **571**, 58–65.
43. Marion, V., Stoetzel, C., Schlicht, D., Messaddeq, N., Koch, M., Flori, E., Danse, J.M., Mandel, J.L. and Dollfus, H. (2009) Transient ciliogenesis involving Bardet-Biedl syndrome proteins is a fundamental characteristic of adipogenic differentiation. *Proc. Natl. Acad. Sci. USA.*, **106**, 1820–1825.
44. Aksanov, O., Green, P. and Birk, R.Z. (2014) BBS4 directly affects proliferation and differentiation of adipocytes. *Cell. Mol. Life Sci.*, **71**, 3381–3392.
45. Duval, C., Thissen, U., Keshtkar, S., Accart, B., Stienstra, R., Boekschoten, M.V., Roskams, T., Kersten, S. and Muller, M. (2010) Adipose tissue dysfunction signals progression of hepatic steatosis towards nonalcoholic steatohepatitis in C57BL/6 mice. *Diabetes*, **59**, 3181–3191.
46. Jang, H.J., Lim, S., Kim, J.M., Yoon, S., Lee, C.Y., Hwang, H.J., Shin, J.W., Shin, K.J., Kim, H.Y., Park, K.I. *et al.* (2020) Glucosylceramide synthase regulates adipo-osteogenic differentiation through synergistic activation of PPARgamma with GlcCer. *FASEB J.*, **34**, 1270–1287.
47. Kohyama-Koganeya, A., Nabetani, T., Miura, M. and Hirabayashi, Y. (2011) Glucosylceramide synthase in the fat body controls energy metabolism in Drosophila. *J. Lipid Res.*, **52**, 1392–1399.
48. Evans, S.E., Kottom, T.J., Pagano, R.E. and Limper, A.H. (2012) Primary alveolar epithelial cell surface membrane microdomain function is required for pneumocystis beta-glucan-induced inflammatory responses. *Innate Immun.*, **18**, 709–716.
49. Cawthorn, W.P. and Sethi, J.K. (2008) TNF-alpha and adipocyte biology. *FEBS Lett.*, **582**, 117–131.
50. Gabriel, T.L., Mirzaian, M., Hooibrink, B., Ottenhoff, R., van Roomen, C., Aerts, J. and van Eijk, M. (2017) Induction of Sphk1 activity in obese adipose tissue macrophages promotes survival. *PLoS One*, **12**, e0182075.
51. Falk, N., Losl, M., Schroder, N. and Giessl, A. (2015) Specialized cilia in mammalian sensory systems. *Cell*, **4**, 500–519.
52. DeMaria, S. and Ngai, J. (2010) The cell biology of smell. *J. Cell Biol.*, **191**, 443–452.
53. Tadenev, A.L., Kulaga, H.M., May-Simera, H.L., Kelley, M.W., Katsanis, N. and Reed, R.R. (2011) Loss of Bardet-Biedl syndrome protein-8 (BBS8) perturbs olfactory function, protein localization, and axon targeting. *Proc. Natl. Acad. Sci. USA.*, **108**, 10320–10325.
54. Seo, S., Mullins, R.F., Dumitrescu, A.V., Bhattarai, S., Gratie, D., Wang, K., Stone, E.M., Sheffield, V. and Drack, A.V. (2013) Subretinal gene therapy of mice with Bardet-Biedl syndrome type 1. *Invest. Ophthalmol. Vis. Sci.*, **54**, 6118–6132.
55. Jiang, J., Promchan, K., Jiang, H., Awasthi, P., Marshall, H., Harned, A. and Natarajan, V. (2016) Depletion of BBS protein LZTFL1 affects growth and causes retinal degeneration in mice. *J. Genet. Genomics*, **43**, 381–391.
56. Abd-El-Barr, M.M., Sykoudis, K., Andrabi, S., Eichers, E.R., Pennesi, M.E., Tan, P.L., Wilson, J.H., Katsanis, N., Lupski, J.R. and Wu, S.M. (2007) Impaired photoreceptor protein transport and synaptic transmission in a mouse model of Bardet-Biedl syndrome. *Vis. Res.*, **47**, 3394–3407.
57. Eichers, E.R., Abd-El-Barr, M.M., Paylor, R., Lewis, R.A., Bi, W., Lin, X., Meehan, T.P., Stockton, D.W., Wu, S.M., Lindsay, E. *et al.* (2006) Phenotypic characterization of Bbs4 null mice reveals age-dependent penetrance and variable expressivity. *Hum. Genet.*, **120**, 211–226.
58. Mykytyn, K., Mullins, R.F., Andrews, M., Chiang, A.P., Swiderski, R.E., Yang, B., Braun, T., Casavant, T., Stone, E.M. and Sheffield, V.C. (2004) Bardet-Biedl syndrome type 4 (BBS4)-null mice implicate Bbs4 in flagella formation but not global cilia assembly. *Proc. Natl. Acad. Sci. USA.*, **101**, 8664–8669.
59. Ross, A.J., May-Simera, H., Eichers, E.R., Kai, M., Hill, J., Jagger, D.J., Leitch, C.C., Chapple, J.P., Munro, P.M., Fisher, S. *et al.* (2005) Disruption of Bardet-Biedl syndrome ciliary proteins perturbs planar cell polarity in vertebrates. *Nat. Genet.*, **37**, 1135–1140.
60. Forsythe, E., Kenny, J., Bacchelli, C. and Beales, P.L. (2018) Managing Bardet-Biedl syndrome-now and in the future. *Front. Pediatr.*, **6**, 23.
61. McIntyre, J.C., Davis, E.E., Joiner, A., Williams, C.L., Tsai, I.C., Jenkins, P.M., McEwen, D.P., Zhang, L., Escobado, J., Thomas, S. *et al.* (2012) Gene therapy rescues cilia defects and restores olfactory function in a mammalian ciliopathy model. *Nat. Med.*, **18**, 1423–1428.
62. Williams, C.L., Uytingco, C.R., Green, W.W., McIntyre, J.C., Ukhanov, K., Zimmerman, A.D., Shively, D.T., Zhang, L., Nishimura, D.Y., Sheffield, V.C. *et al.* (2017) Gene therapeutic reversal of peripheral olfactory impairment in Bardet-Biedl syndrome. *Mol. Ther.*, **25**, 904–916.
63. Simons, D.L., Boye, S.L., Hauswirth, W.W. and Wu, S.M. (2011) Gene therapy prevents photoreceptor death and preserves retinal function in a Bardet-Biedl syndrome mouse model. *Proc. Natl. Acad. Sci. USA.*, **108**, 6276–6281.
64. Chamling, X., Seo, S., Bugge, K., Searby, C., Guo, D.F., Drack, A.V., Rahmouni, K. and Sheffield, V.C. (2013) Ectopic

expression of human BBS4 can rescue Bardet-Biedl syndrome phenotypes in Bbs4 null mice. *PLoS One*, **8**, e59101.
65. Poueymirou, W.T., Auerbach, W., Frendewey, D., Hickey, J.F., Escaravage, J.M., Esau, L., Dore, A.T., Stevens, S., Adams, N.C., Dominguez, M.G. *et al*. (2007) F0 generation mice fully derived from gene-targeted embryonic stem cells allowing immediate phenotypic analyses. *Nat. Biotechnol*., **25**, 91–99.
66. Sardi, S.P., Viel, C., Clarke, J., Treleaven, C.M., Richards, A.M., Park, H., Olszewski, M.A., Dodge, J.C., Marshall, J., Makino, E. *et al*. (2017) Glucosylceramide synthase inhibition alleviates aberrations in synucleinopathy models. *Proc. Natl. Acad. Sci. USA*., **114**, 2699–2704.
67. Rogers, K.A., Moreno, S.E., Smith, L.A., Husson, H., Bukanov, N.O., Ledbetter, S.R., Budman, Y., Lu, Y., Wang, B., Ibraghimov-Beskrovnaya, O. *et al*. (2016) Differences in the timing and magnitude of Pkd1 gene deletion determine the severity of polycystic kidney disease in an orthologous mouse model of ADPKD. *Physiol. Rep*., **4**, e12846.
68. Yang, M. and Crawley, J.N. (2009) Simple behavioral assessment of mouse olfaction. *Curr. Protoc. Neurosci*., Chapter 8, Unit, **8**, 24.
69. Natoli, T.A., Smith, L.A., Rogers, K.A., Wang, B., Komarnitsky, S., Budman, Y., Belenky, A., Bukanov, N.O., Dackowski, W.R., Husson, H. *et al*. (2010) Inhibition of glucosylceramide accumulation results in effective blockade of polycystic kidney disease in mouse models. *Nat. Med*., **16**, 788–792.
70. Humes, H.D., Fissell, W.H., Weitzel, W.F., Buffington, D.A., Westover, A.J., MacKay, S.M. and Gutierrez, J.M. (2002) Metabolic replacement of kidney function in uremic animals with a bioartificial kidney containing human cells. *Am. J. Kidney Dis*., **39**, 1078–1087.
71. Kramer, A., Green, J., Pollard, J., Jr. and Tugendreich, S. (2014) Causal analysis approaches in ingenuity pathway analysis. *Bioinformatics*, **30**, 523–530.
72. Natoli, T.A., Husson, H., Rogers, K.A., Smith, L.A., Wang, B., Budman, Y., Bukanov, N.O., Ledbetter, S.R., Klinger, K.W., Leonard, J.P. *et al*. (2012) Loss of GM3 synthase gene, but not sphingosine kinase 1, is protective against murine nephronophthisis-related polycystic kidney disease. *Hum. Mol. Genet*., **21**, 3397–3407.
73. Husson, H., Moreno, S., Smith, L.A., Smith, M.M., Russo, R.J., Pitstick, R., Sergeev, M., Ledbetter, S.R., Bukanov, N.O., Lane, M. *et al*. (2016) Reduction of ciliary length through pharmacologic or genetic inhibition of CDK5 attenuates polycystic kidney disease in a model of nephronophthisis. *Hum. Mol. Genet*., **25**, 2245–2255.